

## **Supporting Information**

**The effects of metal cofactors on the reactivity of quercetin 2,4-dioxygenase: synthetic model studies with M(II)-complexes (M = Mn, Co, Ni, Cu, Zn) and assessment of the regulatory factors in catalytic efficacy**

Nirmalya Podder and Sukanta Mandal\*

Department of Chemistry, Indian Institute of Technology Kharagpur, Kharagpur-721302, India.

Email: [sukanta.mandal@chem.iitkgp.ac.in](mailto:sukanta.mandal@chem.iitkgp.ac.in)

<b>Table of contents</b>	<b>Page no.</b>
Table S1	S3
Table S2, Scheme S1	S4
Figure S1, Figure S2	S5
Figure S3, Figure S4	S6
Figure S5, Figure S6	S7
Figure S7, Figure S8	S8
Figure S9, Figure S10	S9
Figure S11, Figure S12, Figure S13	S10
Figure S14, Figure S15, Figure S16	S11
Figure S17, Figure S18, Figure S19	S12
Figure S20, Figure S21	S13
Figure S22, Figure S23	S14
Figure S24, Figure S25	S15
Figure S26, Figure S27, Figure S28	S16
Figure S29, Figure S30, Figure S31	S17
Figure S32, Figure S33, Figure S34	S18
Figure S35, Figure S36	S19
Figure S37, Figure S38, Table S3	S20
Figure S39	S21
Figure S40, Table S4, Table S5	S22
Table S6, Table S7, Table S8	S23
Figure S41, Figure S42, Figure S43	S24
Figure S44	S25
Figure S45, Figure S46	S26

**Table S1.** Data collection and structure refinement parameters for **2<sup>OAc</sup>·2H<sub>2</sub>O**, **3<sup>OAc</sup>**, **4<sup>OAc</sup>·CH<sub>2</sub>Cl<sub>2</sub>·2H<sub>2</sub>O** and **5<sup>OAc</sup>·2H<sub>2</sub>O**

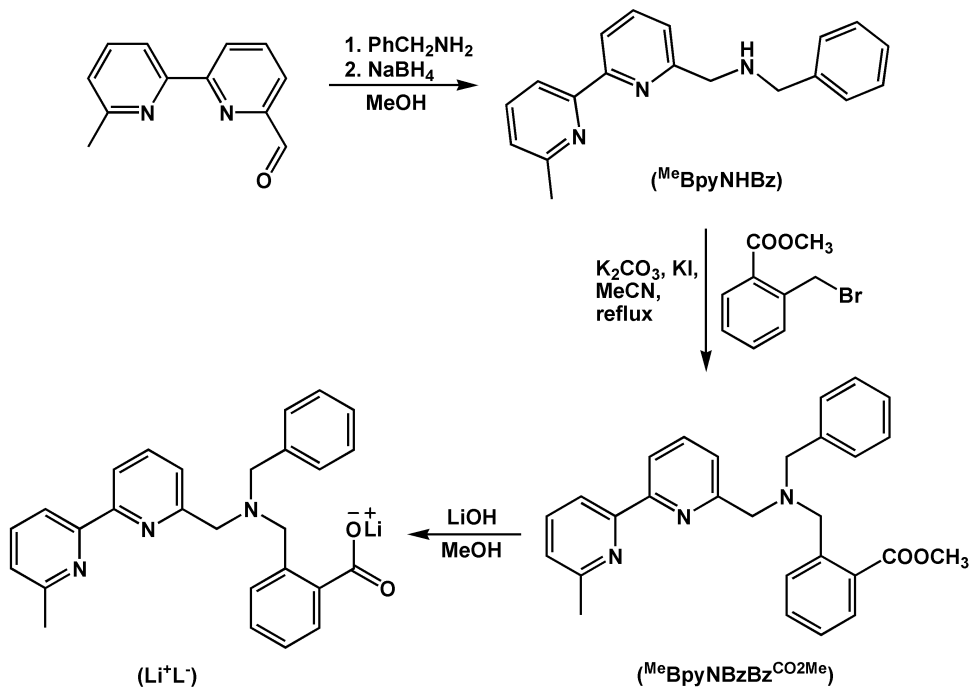
	<b>2<sup>OAc</sup>·2H<sub>2</sub>O</b>	<b>3<sup>OAc</sup></b>	<b>4<sup>OAc</sup>·CH<sub>2</sub>Cl<sub>2</sub>·2H<sub>2</sub>O</b>	<b>5<sup>OAc</sup>·2H<sub>2</sub>O</b>
CCDC	2203838	2203839	2203840	2203841
Chemical formula	C <sub>29</sub> H <sub>31</sub> CoN <sub>3</sub> O <sub>6</sub>	C <sub>29</sub> H <sub>27</sub> N <sub>3</sub> NiO <sub>4</sub>	C <sub>30</sub> H <sub>33</sub> Cl <sub>2</sub> CuN <sub>3</sub> O <sub>6</sub>	C <sub>29</sub> H <sub>31</sub> N <sub>3</sub> O <sub>6</sub> Zn
Formula weight	576.51	540.23	666.04	582.96
Temperature (K)	296(2)	296(2)	296(2)	296(2)
$\lambda$ (Å)	Mo-K $\alpha$ (0.71073)	Mo-K $\alpha$ (0.71073)	Mo-K $\alpha$ (0.71073)	Mo-K $\alpha$ (0.71073)
Crystal system	Monoclinic	Monoclinic	Monoclinic	Monoclinic
Space group	P2 <sub>1</sub> /n (no. 14)			
<i>a</i> (Å)	14.39(4)	10.867(2)	9.119(2)	14.27(5)
<i>b</i> (Å)	12.93(4)	14.873(3)	32.781(7)	12.90(4)
<i>c</i> (Å)	15.07(4)	15.935(3)	9.975(2)	15.06(5)
$\alpha$ (°)	90	90	90	90
$\beta$ (°)	93.42(5)	96.014(6)	104.32(3)	92.99(5)
$\gamma$ (°)	90	90	90	90
<i>V</i> (Å <sup>3</sup> )	2799(14)	2561.3(8)	2889.2(11)	2769(16)
<i>Z</i>	4	4	4	4
<i>D<sub>c</sub></i> (g cm <sup>-3</sup> )	1.359	1.401	1.531	1.389
$\mu$ (mm <sup>-1</sup> )	0.659	0.798	0.991	0.934
Reflections measured	23137	23495	42404	18403
Unique reflections [ <i>R</i> <sub>int</sub> ]	7334 [0.0608]	4781 [0.1510]	8746 [0.0355]	4430 [0.1124]
Number of reflections used [ <i>I</i> > 2 $\sigma$ ( <i>I</i> )]	4444	2401	7257	2386
Number of parameters	361	335	395	370
Final R indices	<sup>a</sup> <i>R</i> <sub>1</sub> = 0.0522; <sup>b</sup> <i>wR</i> <sub>2</sub> = 0.1440	<sup>a</sup> <i>R</i> <sub>1</sub> = 0.0730; <sup>b</sup> <i>wR</i> <sub>2</sub> = 0.1645	<sup>a</sup> <i>R</i> <sub>1</sub> = 0.0403; <sup>b</sup> <i>wR</i> <sub>2</sub> = 0.1079	<sup>a</sup> <i>R</i> <sub>1</sub> = 0.0567; <sup>b</sup> <i>wR</i> <sub>2</sub> = 0.1224
R indices (all data)	<sup>a</sup> <i>R</i> <sub>1</sub> = 0.0984; <sup>b</sup> <i>wR</i> <sub>2</sub> = 0.1794	<sup>a</sup> <i>R</i> <sub>1</sub> = 0.1558; <sup>b</sup> <i>wR</i> <sub>2</sub> = 0.2085	<sup>a</sup> <i>R</i> <sub>1</sub> = 0.0512; <sup>b</sup> <i>wR</i> <sub>2</sub> = 0.1125	<sup>a</sup> <i>R</i> <sub>1</sub> = 0.1243; <sup>b</sup> <i>wR</i> <sub>2</sub> = 0.1489
Goodness-of-fit on <i>F</i> <sup>2</sup>	1.004	0.953	1.005	0.994
Largest residual peak and hole (e.Å <sup>-3</sup> )	0.318 and -0.546	0.508 and -0.404	0.528 and -1.011	0.294 and -0.266

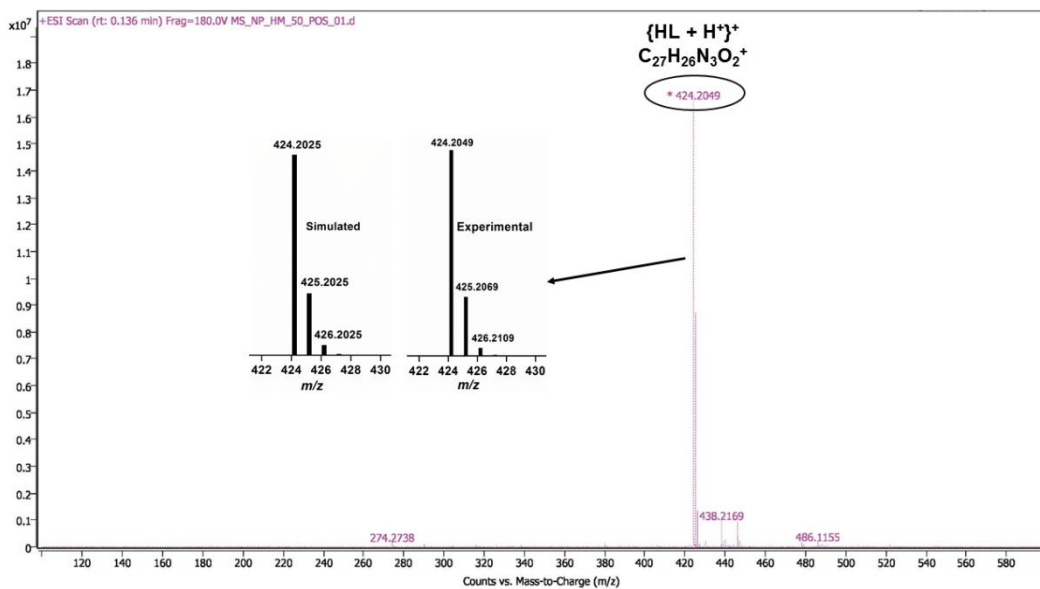
$$^aR_1 = \sum(|F_o| - |F_c|)/\sum|F_o|, ^bR_2 = \{\sum[w(|F_o|^2 - |F_c|^2)^2]/\sum[w(|F_o|^2)^2]\}^{1/2}.$$

**Table S2.** Data collection and structure refinement parameters for **2<sup>fla</sup>·MeOH**

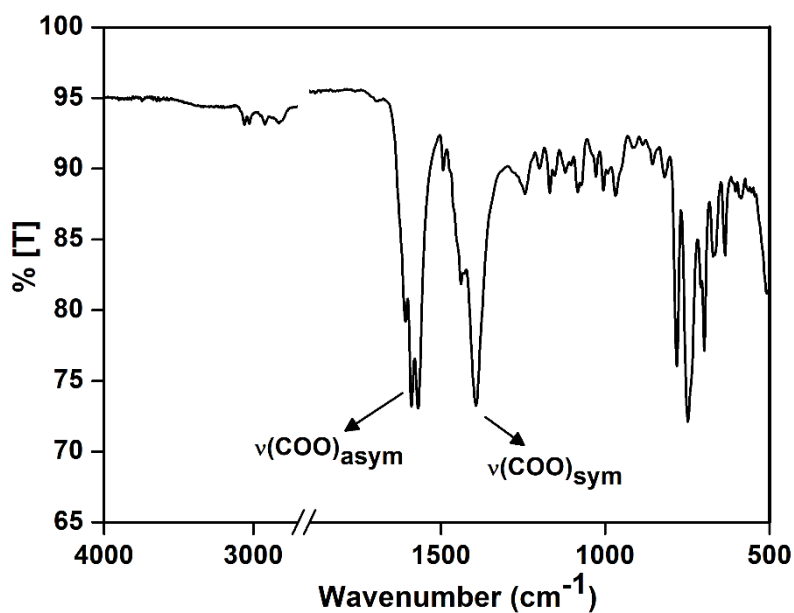
	<b>2<sup>fla</sup>·MeOH</b>
CCDC	2203842
Chemical formula	C <sub>43</sub> H <sub>37</sub> CoN <sub>3</sub> O <sub>6</sub>
Formula weight	750.70
Temperature (K)	296(2)
$\lambda$ (Å)	Mo-K $\alpha$ (0.71073)
Crystal system	Monoclinic
Space group	P2 <sub>1</sub> /c (no. 14)
<i>a</i> (Å)	9.5859(16)
<i>b</i> (Å)	36.019(4)
<i>c</i> (Å)	10.7112(19)
$\alpha$ (°)	90
$\beta$ (°)	92.771(18)
$\gamma$ (°)	90
<i>V</i> (Å <sup>3</sup> )	3694.0(10)
<i>Z</i>	4
<i>D</i> <sub>c</sub> (g cm <sup>-3</sup> )	1.348
$\mu$ (mm <sup>-1</sup> )	0.518
Reflections measured	43045
Unique reflections [ <i>R</i> <sub>int</sub> ]	9094 [0.0952]
Number of reflections used [ <i>I</i> > 2 $\sigma$ ( <i>I</i> )]	3694
Number of parameters	479
Final R indices	<sup>a</sup> <i>R</i> <sub>1</sub> = 0.0605; <sup>b</sup> <i>wR</i> <sub>2</sub> = 0.1342
R indices (all data)	<sup>a</sup> <i>R</i> <sub>1</sub> = 0.1723; <sup>b</sup> <i>wR</i> <sub>2</sub> = 0.1863
Goodness-of-fit on <i>F</i> <sup>2</sup>	0.995
Largest residual peak and hole (e.Å <sup>-3</sup> )	0.322 and -0.274

<sup>a</sup>*R*<sub>1</sub> =  $\Sigma(|F_o| - |F_c|)/\Sigma|F_o|$ . <sup>b</sup>*wR*<sub>2</sub> = { $\Sigma[w(|F_o|^2 - |F_c|^2)^2]/\Sigma[w(|F_o|^2)^2]$ }<sup>1/2</sup>.

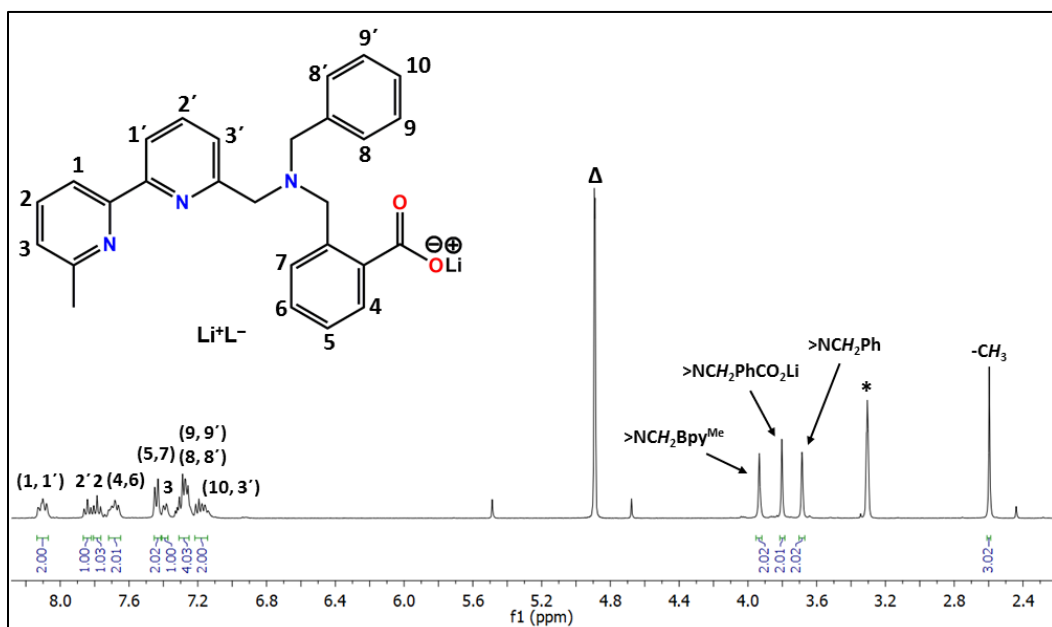
**Scheme S1.** Synthetic route of the ligand Li<sup>+</sup>L<sup>-</sup>.



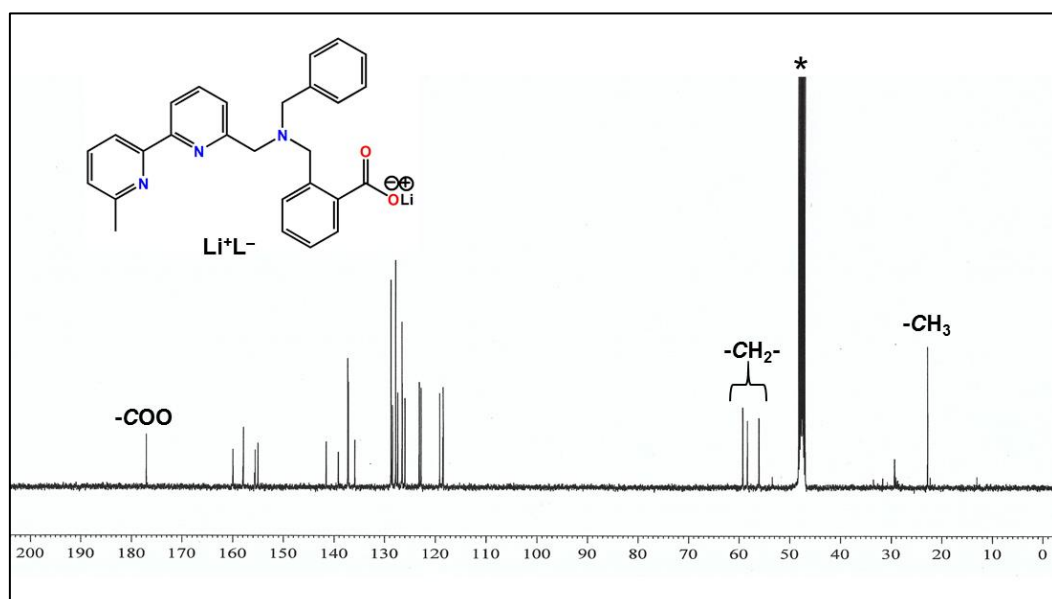
**Figure S1.** ESI(+)–MS spectrum of the lithium salt of ligand  $L^-$  in methanol with a trace quantity of HCOOH.



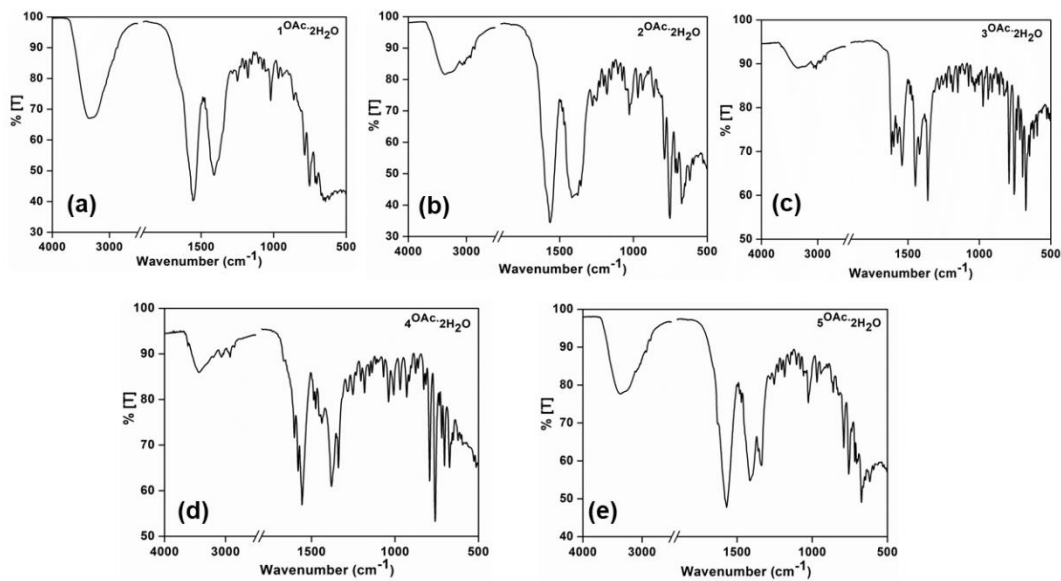
**Figure S2.** ATR-FTIR spectrum (solid sample) of the lithium salt of ligand  $L^-$ .



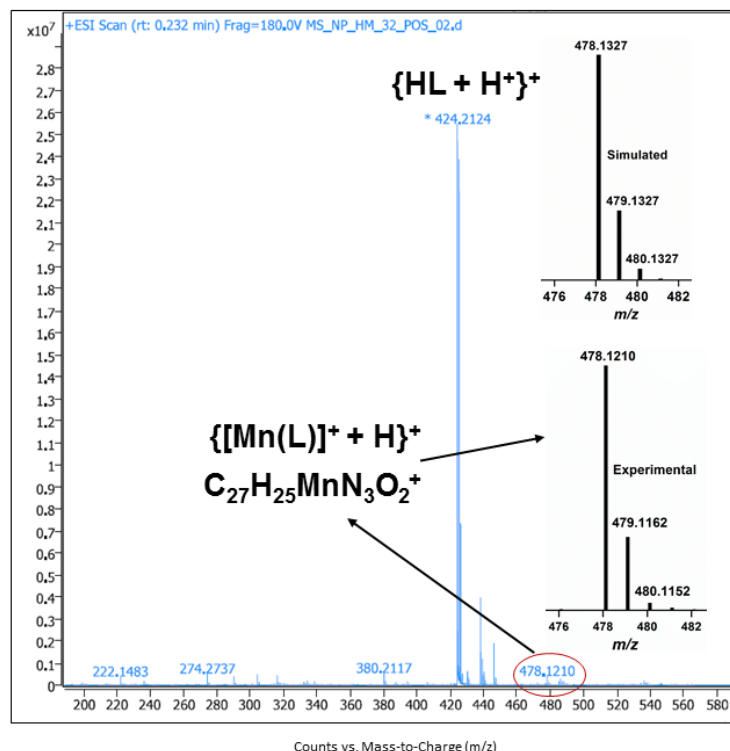
**Figure S3.**  $^1\text{H}$  NMR (400 MHz,  $\text{CD}_3\text{OD}$ , 300 K) spectrum of the ligand  $\text{Li}^+\text{L}^-$ . Symbols ( $\Delta$ ) and (\*) denote water and solvent residual peaks, respectively.



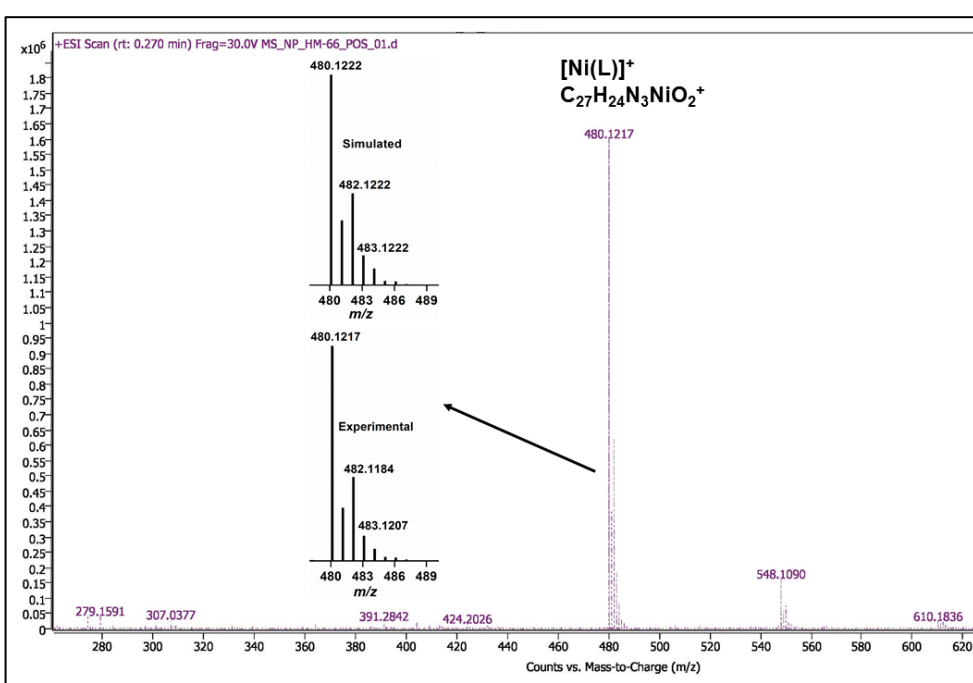
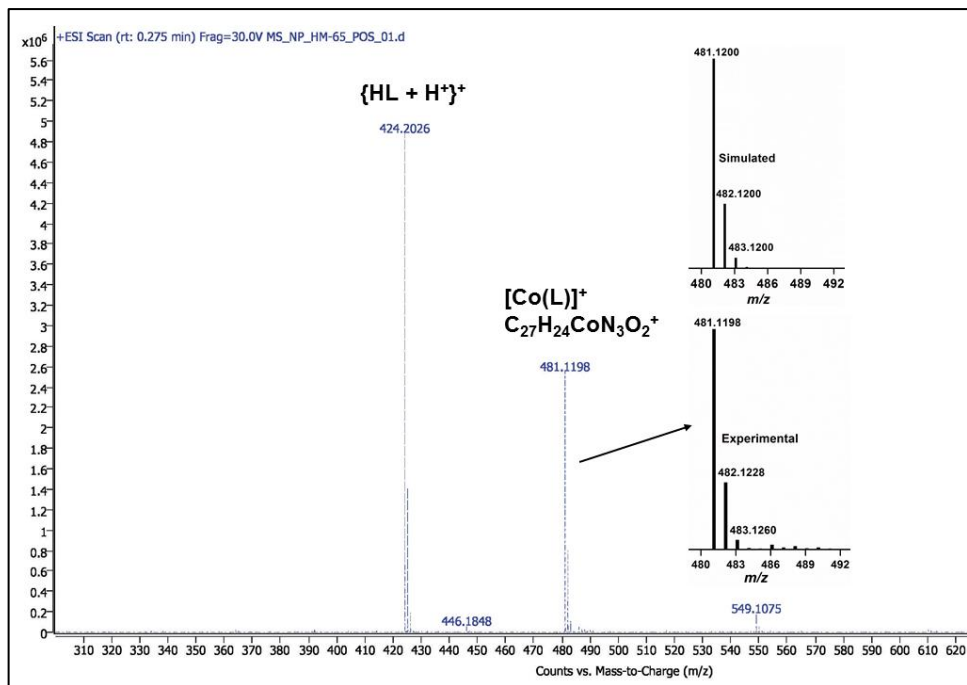
**Figure S4.**  $^{13}\text{C}\{^1\text{H}\}$  NMR (125 MHz,  $\text{CD}_3\text{OD}$ , 300 K) spectrum of the ligand  $\text{Li}^+\text{L}^-$ . The (\*) symbol denotes the solvent residual peak.

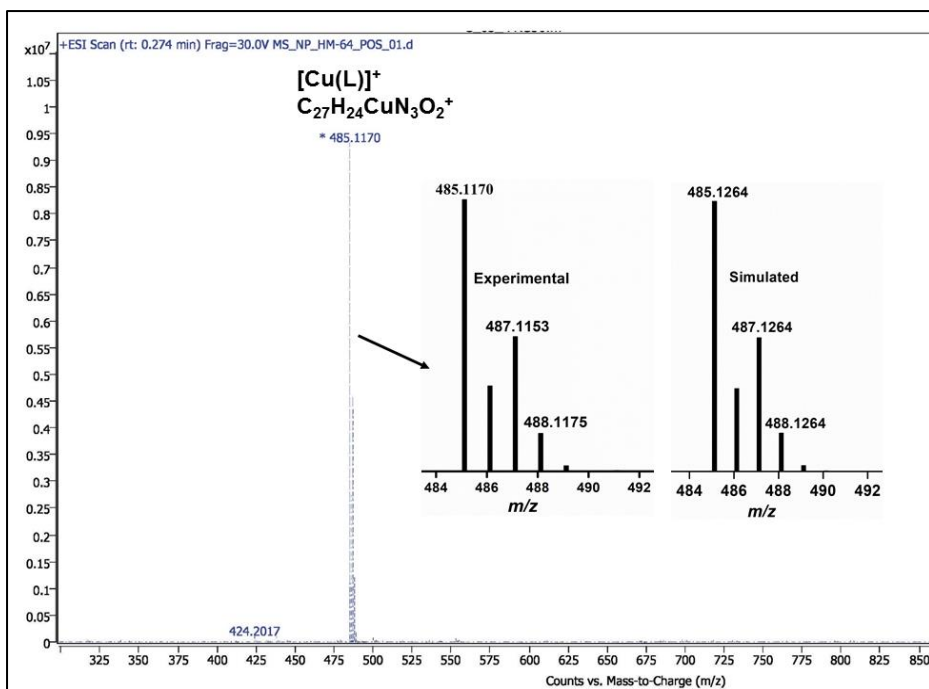


**Figure S5.** ATR-FTIR spectra (solid samples) of acetate-bound metal(II) complexes: (a)  $[\text{Mn}(\text{L})(\text{OAc})] \cdot 2\text{H}_2\text{O}$  (**1<sup>0</sup>Ac·2H<sub>2</sub>O**); (b)  $[\text{Co}(\text{L})(\text{OAc})] \cdot 2\text{H}_2\text{O}$  (**2<sup>0</sup>Ac·2H<sub>2</sub>O**); (c)  $[\text{Ni}(\text{L})(\text{OAc})] \cdot 2\text{H}_2\text{O}$  (**3<sup>0</sup>Ac·2H<sub>2</sub>O**), (d)  $[\text{Cu}(\text{L})(\text{OAc})] \cdot 2\text{H}_2\text{O}$  (**4<sup>0</sup>Ac·2H<sub>2</sub>O**) and  $[\text{Zn}(\text{L})(\text{OAc})] \cdot 2\text{H}_2\text{O}$  (**5<sup>0</sup>Ac·2H<sub>2</sub>O**).

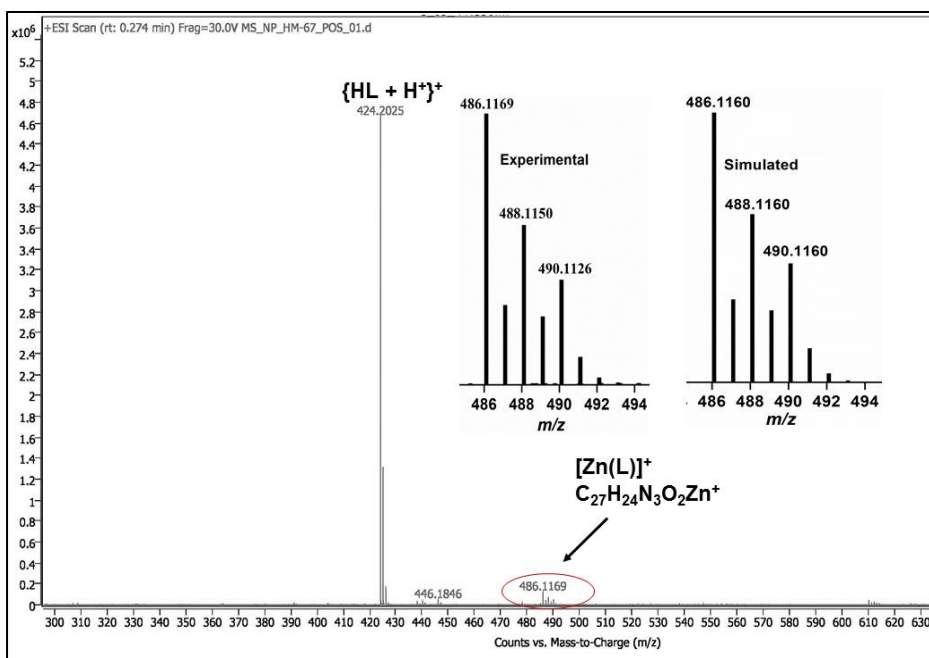


**Figure S6.** ESI(+) MS spectrum of  $[\text{Mn}(\text{L})(\text{OAc})]$  (**1<sup>0</sup>Ac**) in methanol with a trace quantity of HCOOH.

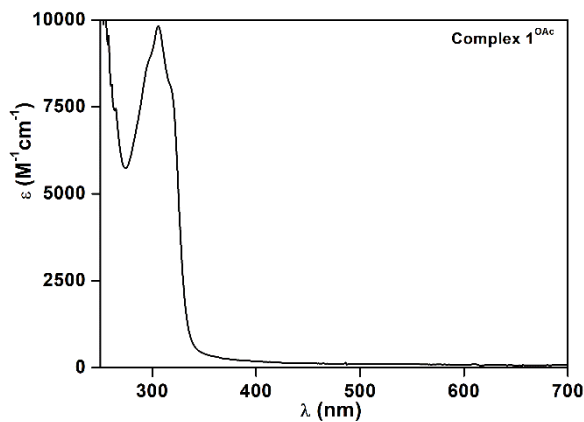




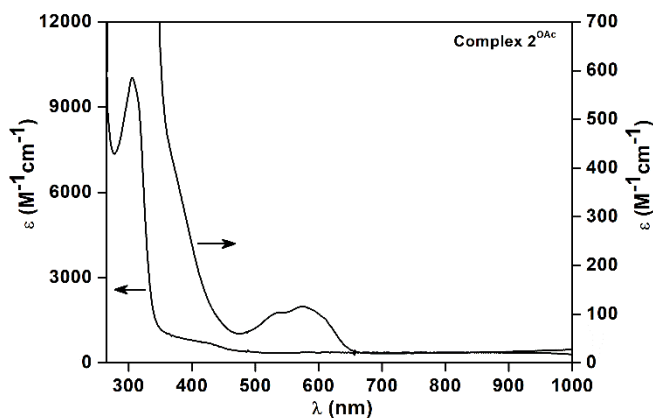
**Figure S9.** ESI(+)-MS spectrum of  $[\text{Cu}(\text{L})(\text{OAc})]$  (**4<sup>OAc</sup>**) in methanol with a trace quantity of HCOOH.



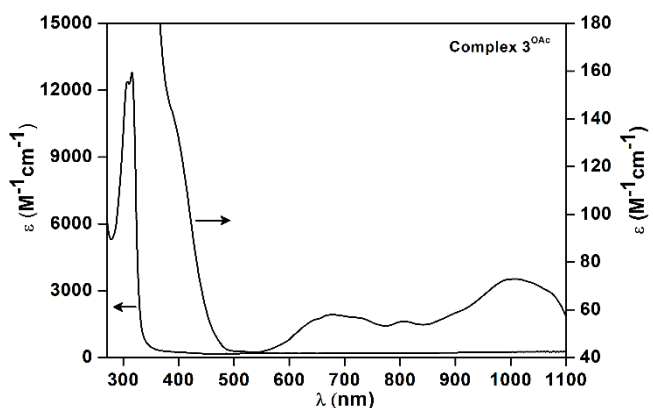
**Figure S10.** ESI(+)-MS spectrum of  $[\text{Zn}(\text{L})(\text{OAc})]$  (**5<sup>OAc</sup>**) in methanol with a trace quantity of HCOOH.



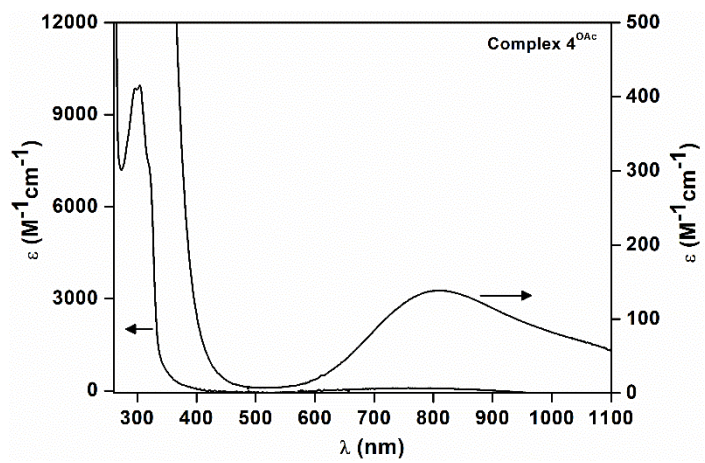
**Figure S11.** UV-vis spectrum of complex  $[Mn(L)(OAc)]$  ( $1^{OAc}$ ) in DMF.



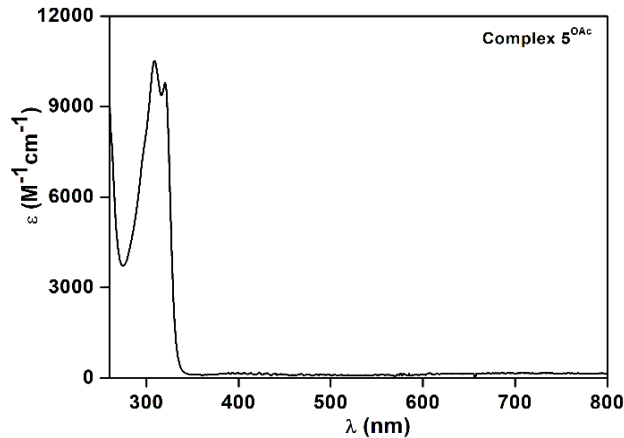
**Figure S12.** UV-vis spectrum of complex  $[Co(L)(OAc)]$  ( $2^{OAc}$ ) in DMF.



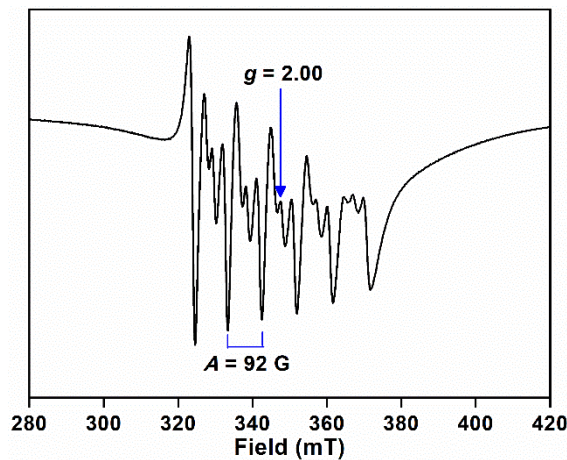
**Figure S13.** UV-vis spectrum of complex  $[Ni(L)(OAc)]$  ( $3^{OAc}$ ) in DMF.



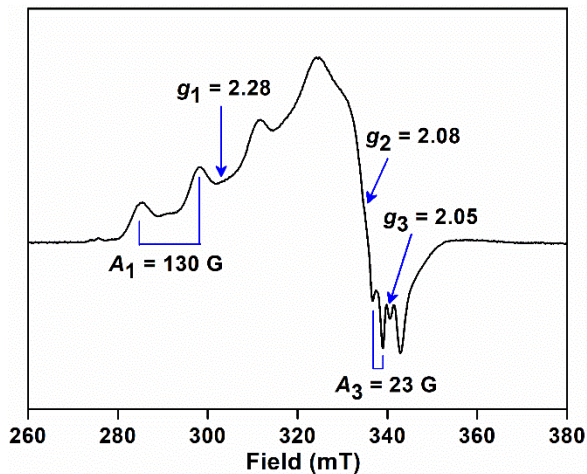
**Figure S14.** UV-vis spectrum of complex  $[\text{Cu}(\text{L})(\text{OAc})]$  ( $\mathbf{4}^{\text{OAc}}$ ) in DMF.



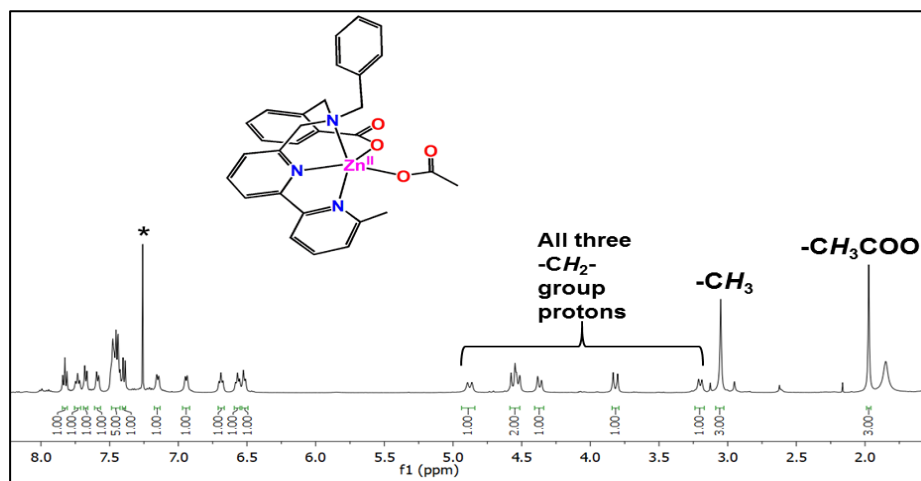
**Figure S15.** UV-vis spectrum of complex  $[\text{Zn}(\text{L})(\text{OAc})]$  ( $\mathbf{5}^{\text{OAc}}$ ) in DMF.



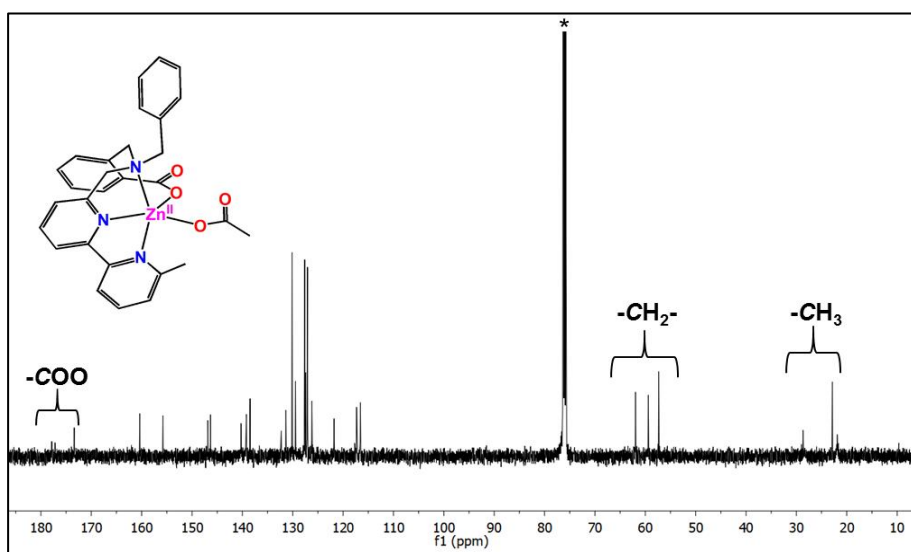
**Figure S16.** X-band EPR spectrum of complex  $[\text{Mn}(\text{L})(\text{OAc})]$  ( $\mathbf{1}^{\text{OAc}}$ ) in DMF at 6 K (microwave frequency  $\approx$  9.72 GHz).



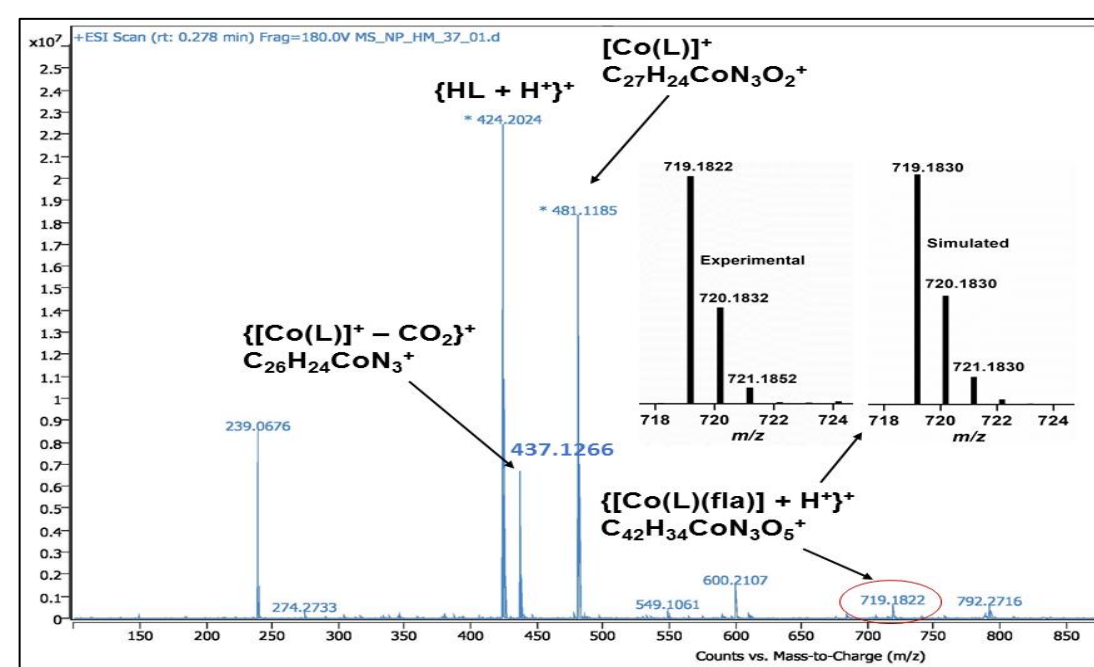
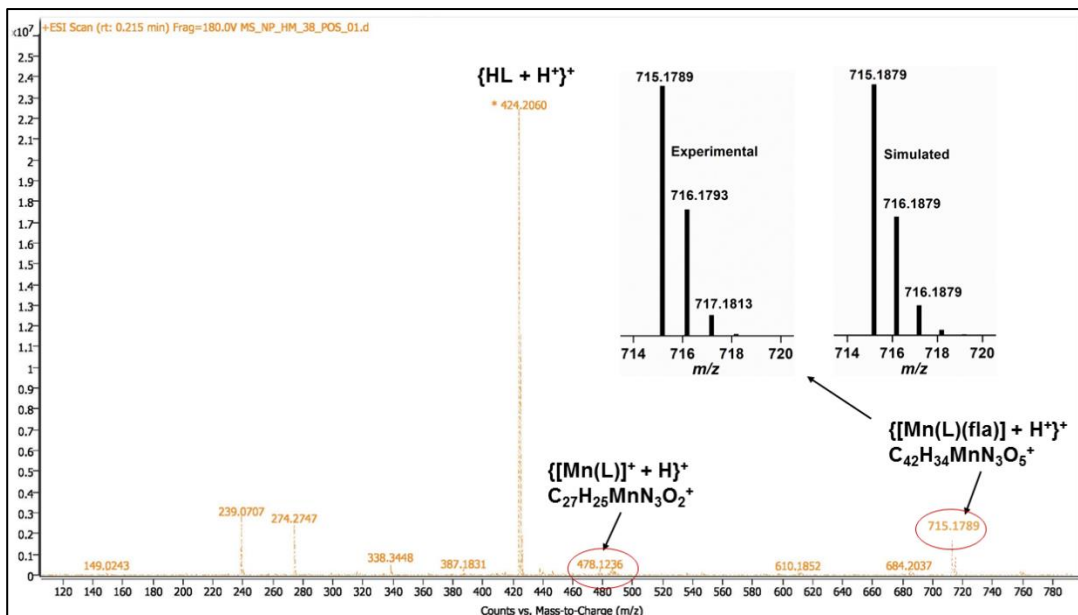
**Figure S17.** X-band EPR spectrum of complex  $[\text{Cu}(\text{L})(\text{OAc})]$  (**4<sup>OAc</sup>**) in DMF at 6 K (microwave frequency  $\approx 9.73$  GHz).



**Figure S18.**  $^1\text{H}$  NMR spectrum (400 MHz, 300 K) of complex  $[\text{Zn}(\text{L})(\text{OAc})]$  (**5**<sup>0Ac</sup>) in  $\text{CDCl}_3$ . The (\*) symbol denotes the solvent residual peak.



**Figure S19.**  $^{13}\text{C}\{\text{H}\}$  NMR spectrum (125 MHz, 300 K) of complex  $[\text{Zn}(\text{L})(\text{OAc})]$  (**5<sup>OAc</sup>**) in  $\text{CDCl}_3$ . The (\*) symbol denotes the solvent residual peak.



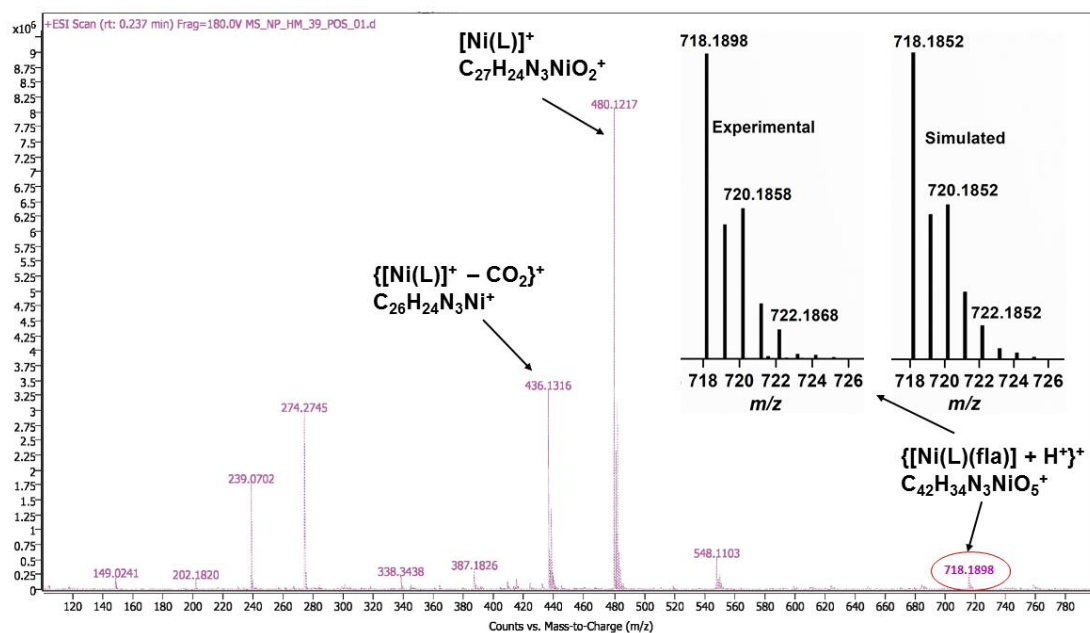


**Figure S22.** ESI(+)-MS spectrum of  $[\text{Ni}(\text{L})(\text{fla})]$  ( $3^{\text{fla}}$ ) in methanol with a trace quantity of HCOOH.

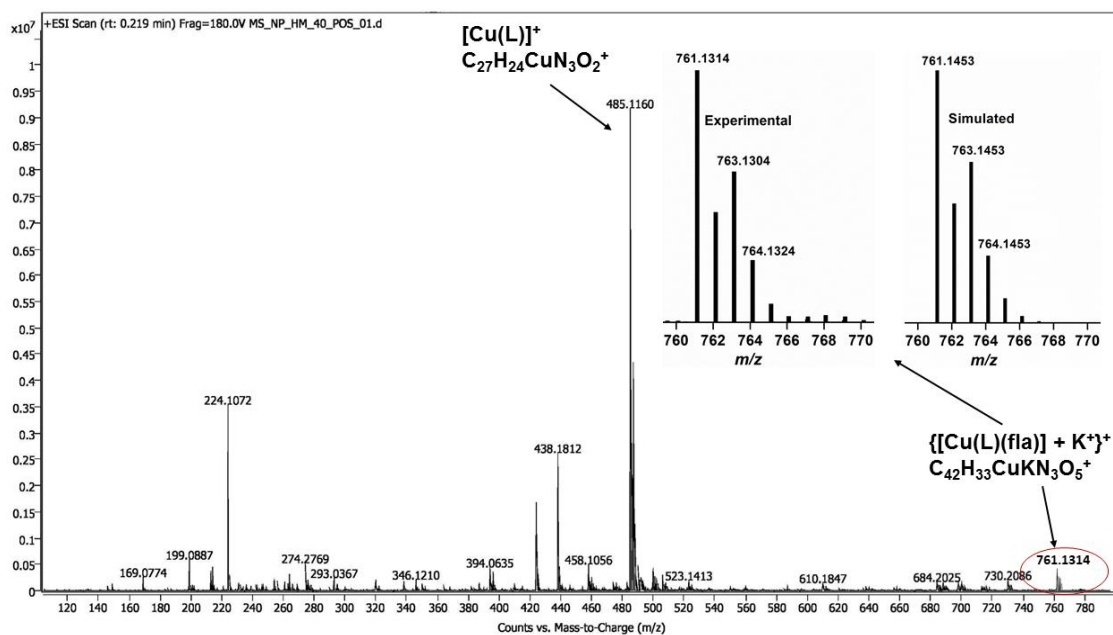


**Figure S23.** ESI(+)-MS spectrum of  $[\text{Cu}(\text{L})(\text{fla})]$  ( $4^{\text{fla}}$ ) in methanol with a trace quantity of HCOOH.

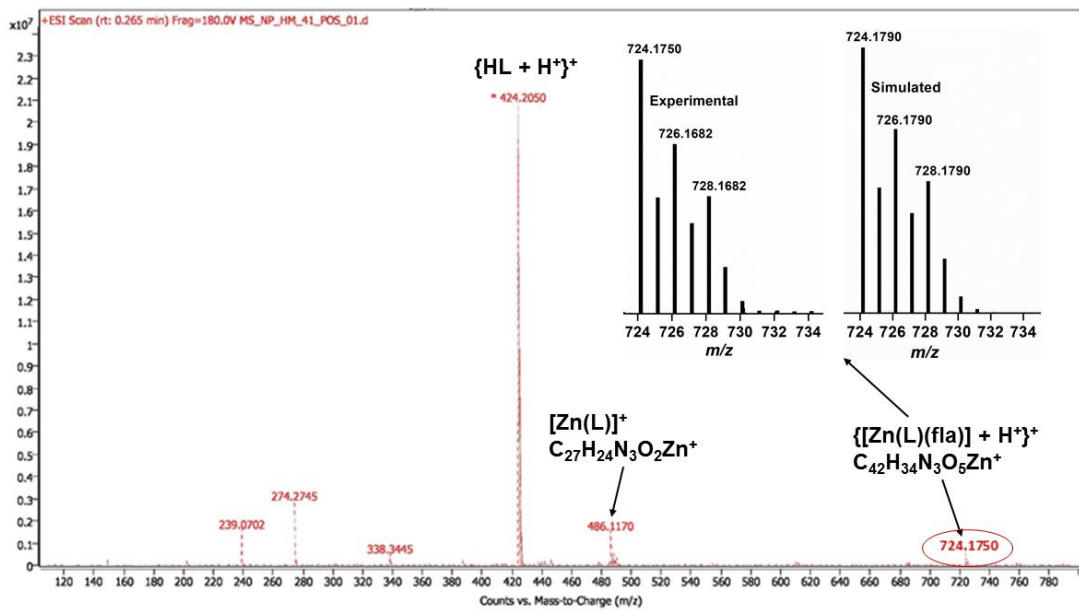


**Figure S24.** ESI(+)–MS spectrum of  $[Zn(L)(fla)]$  ( $5^{fla}$ ) in methanol with a trace quantity of HCOOH.

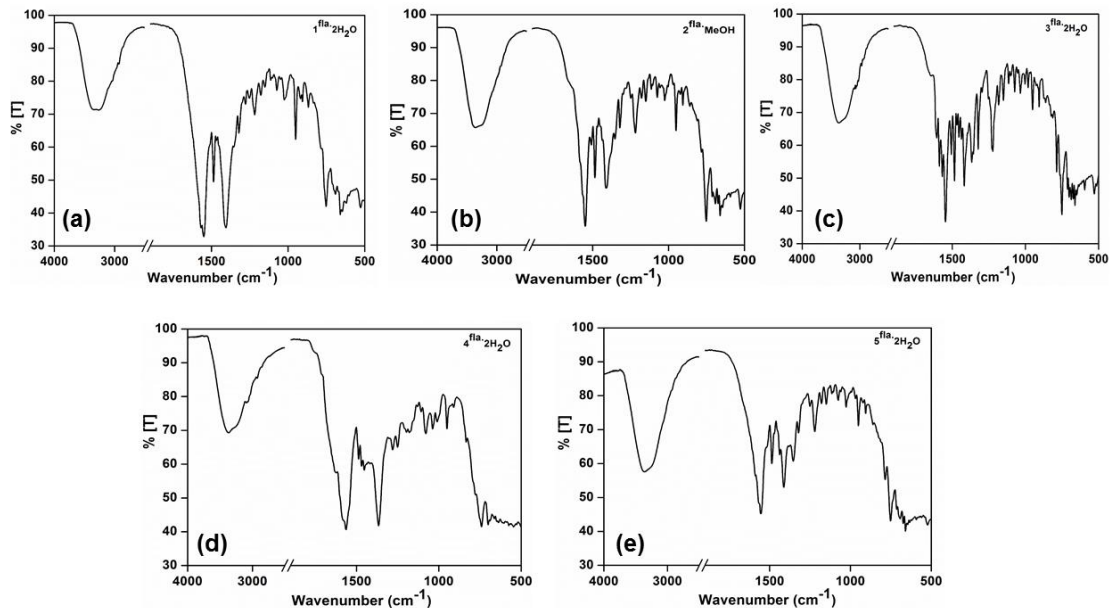


**Figure S25.** ATR-FTIR spectra (solid samples) of the flavonolate-bound metal(II) complexes: (a)  $[\text{Mn}(L)(fla)]\cdot 2\text{H}_2\text{O}$  ( $1^{fla}\cdot 2\text{H}_2\text{O}$ ); (b)  $[\text{Co}(L)(fla)]\cdot \text{MeOH}$  ( $2^{fla}\cdot \text{MeOH}$ ); (c)  $[\text{Ni}(L)(fla)]\cdot 2\text{H}_2\text{O}$  ( $3^{fla}\cdot 2\text{H}_2\text{O}$ ), (d)  $[\text{Cu}(L)(fla)]\cdot 2\text{H}_2\text{O}$  ( $4^{fla}\cdot 2\text{H}_2\text{O}$ ) and  $[Zn(L)(fla)]\cdot 2\text{H}_2\text{O}$  ( $5^{fla}\cdot 2\text{H}_2\text{O}$ ).

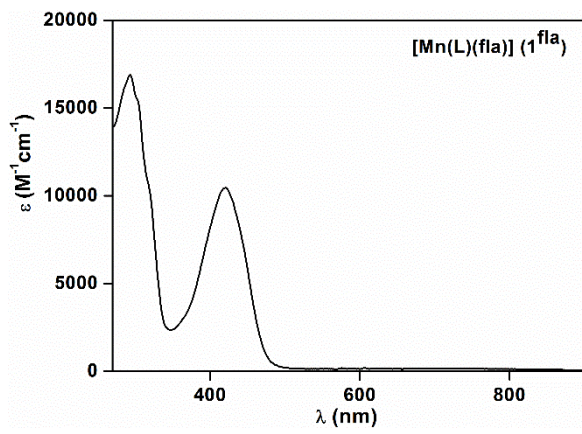


**Figure S26.** UV-vis spectrum of complex  $[\text{Mn}(\text{L})(\text{fla})]$  ( $\mathbf{1}^{\text{fla}}$ ) in DMF.

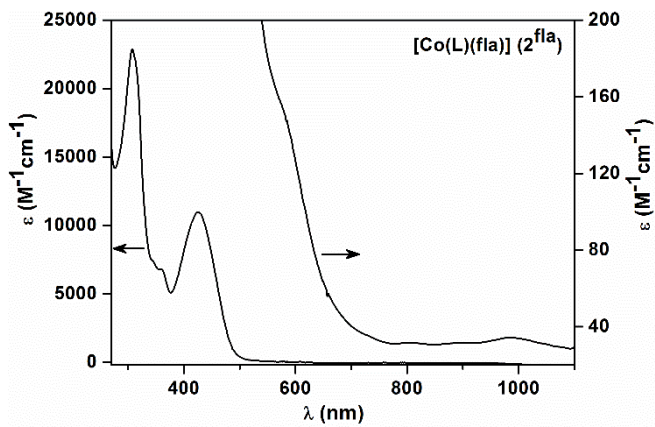


**Figure S27.** UV-vis spectrum of complex  $[\text{Co}(\text{L})(\text{fla})]$  ( $\mathbf{2}^{\text{fla}}$ ) in DMF.

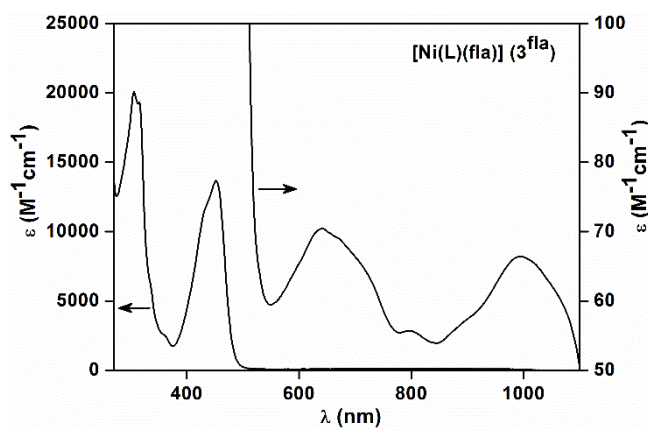


**Figure S28.** UV-vis spectrum of complex  $[\text{Ni}(\text{L})(\text{fla})]$  ( $\mathbf{3}^{\text{fla}}$ ) in DMF.

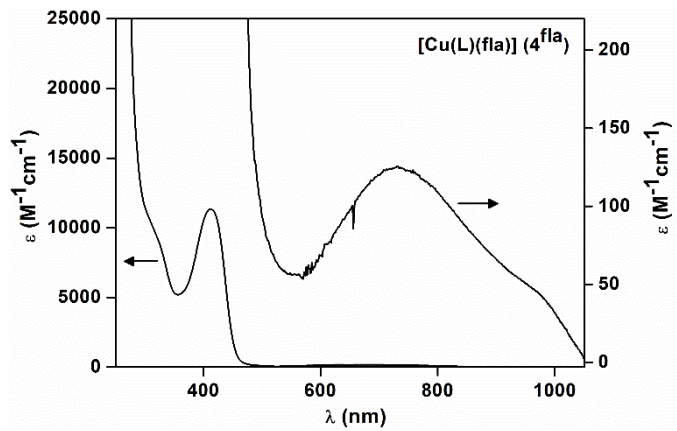


**Figure S29.** UV-vis spectrum of complex  $[\text{Cu}(\text{L})(\text{fla})]$  ( $\mathbf{4}^{\text{fla}}$ ) in DMF.

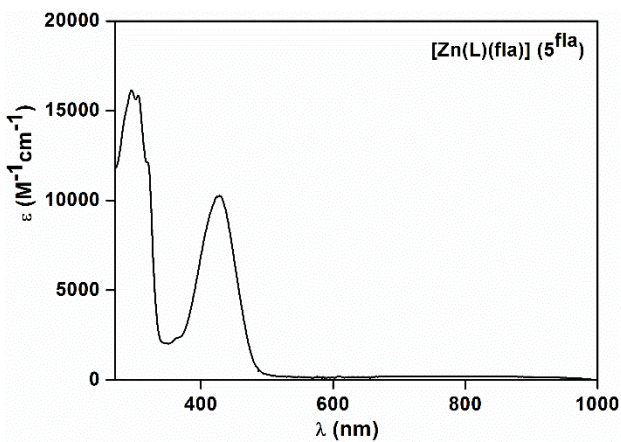


**Figure S30.** UV-vis spectrum of complex  $[\text{Zn}(\text{L})(\text{fla})]$  ( $\mathbf{5}^{\text{fla}}$ ) in DMF.

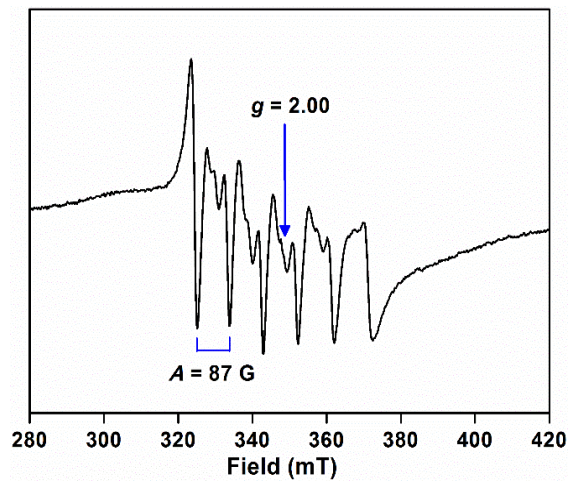


**Figure S31.** X-band EPR spectrum of complex  $[\text{Mn}(\text{L})(\text{fla})]$  ( $\mathbf{1}^{\text{fla}}$ ) in DMF at 6 K (microwave frequency  $\approx 9.74$  GHz).

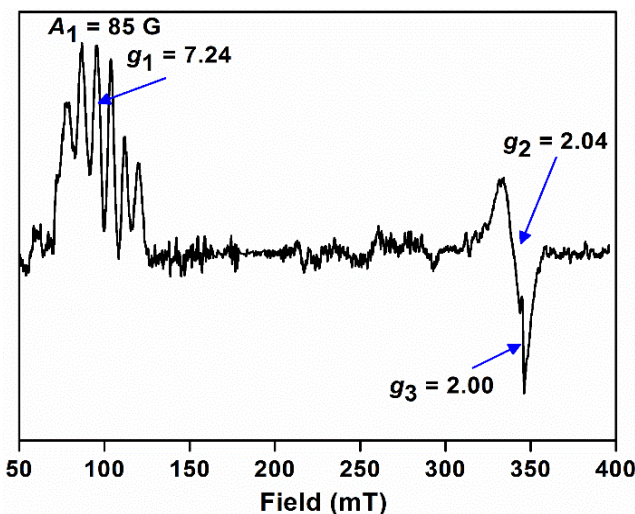


**Figure S32.** X-band EPR spectrum of complex  $[\text{Co}(\text{L})(\text{fla})]$  ( $2^{\text{fla}}$ ) in DMF at 14 K (microwave frequency  $\approx 9.68$  GHz).

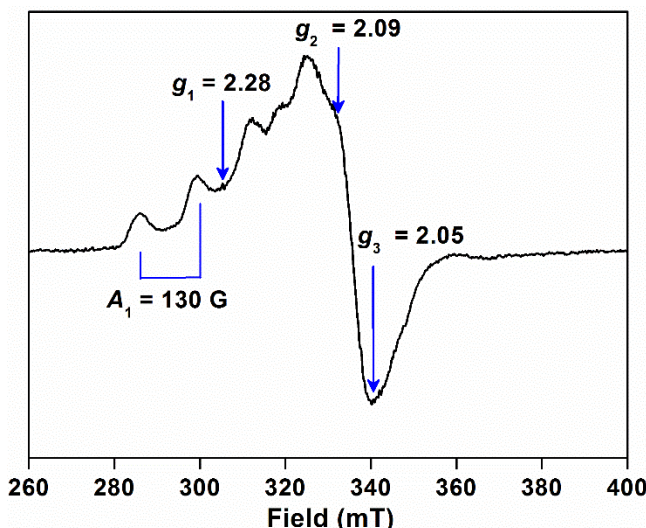


**Figure S33.** X-band EPR spectrum of complex  $[\text{Cu}(\text{L})(\text{fla})]$  ( $4^{\text{fla}}$ ) in DMF at 6 K (microwave frequency  $\approx 9.74$  GHz).

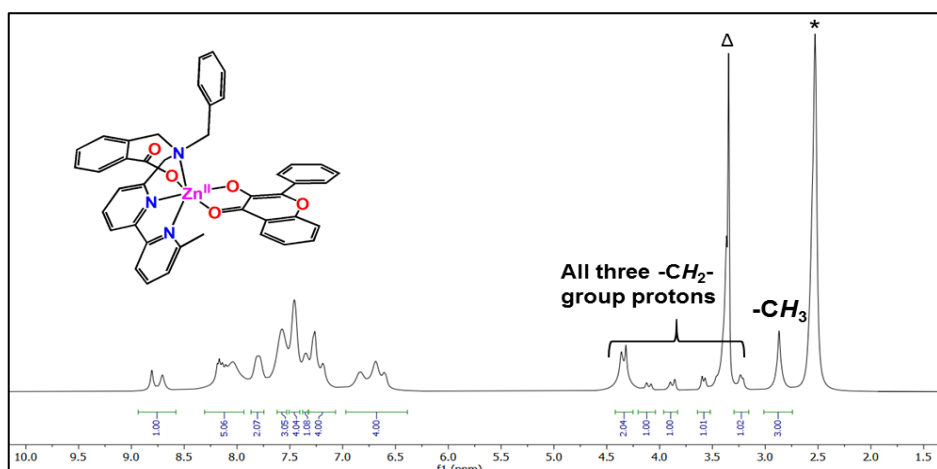


**Figure S34.**  $^1\text{H}$  NMR (400 MHz,  $\text{DMSO}-d_6$ , 300 K) spectrum of complex  $[\text{Zn}(\text{L})(\text{fla})]$  ( $5^{\text{fla}}$ ). Symbols ( $\Delta$ ) and (\*) denote water and solvent residual peaks, respectively.

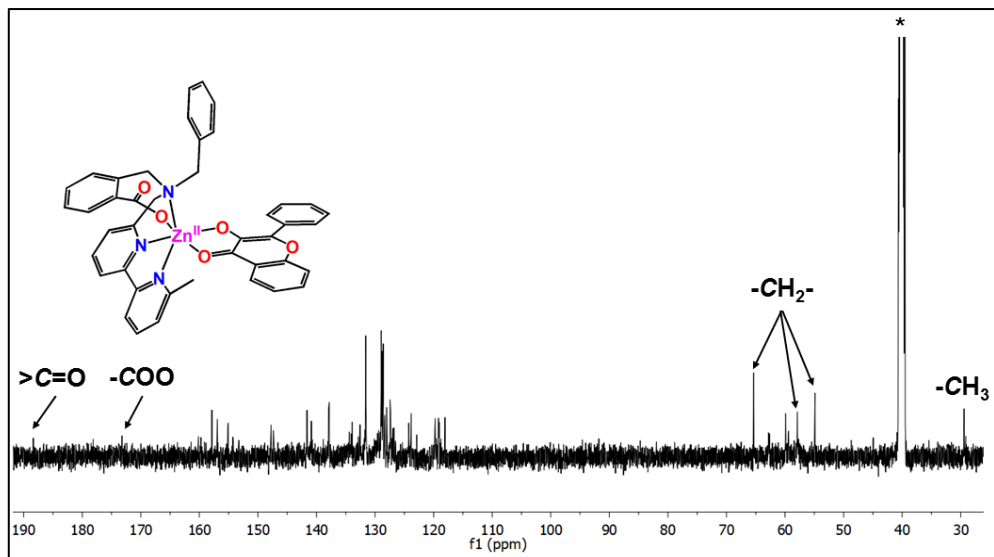


**Figure S35.**  $^{13}\text{C}\{^1\text{H}\}$  NMR (125 MHz,  $\text{DMSO}-d_6$ , 300 K) spectrum of complex  $[\text{Zn}(\text{L})(\text{fla})]$  ( $5^{\text{fla}}$ ). Symbol (\*) represents the solvent residual peak.

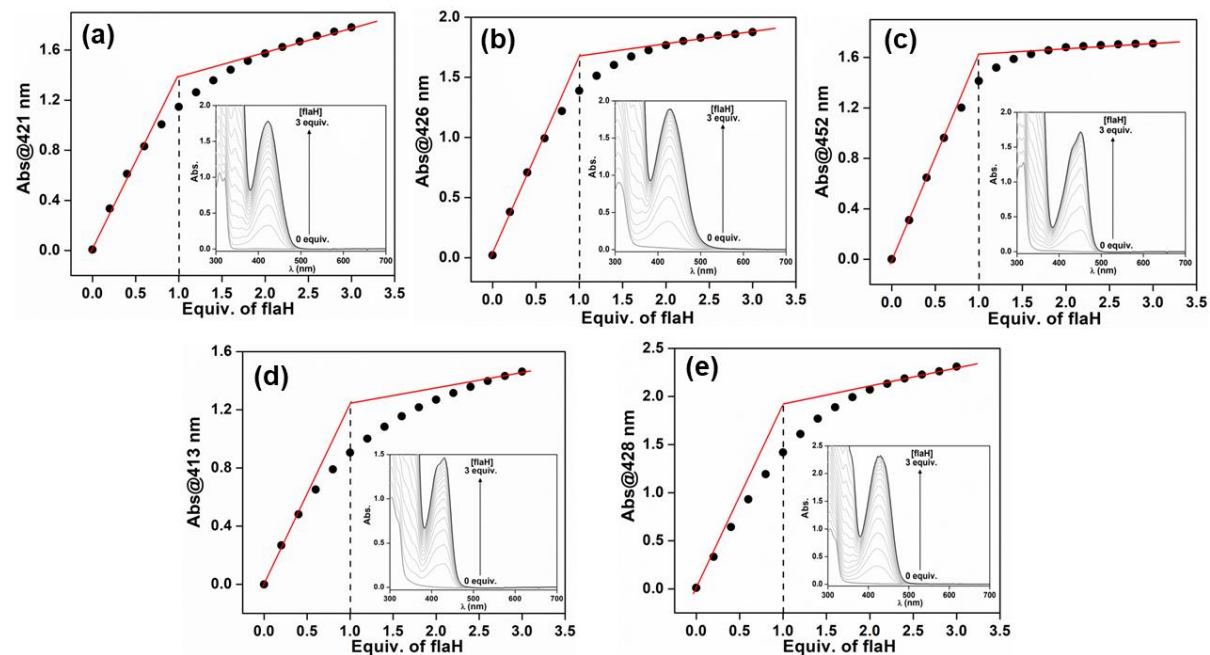


**Figure S36.** Spectrophotometric titration curves of the formation of M(II)-flavonolato adducts upon addition of flavonol into the DMF solution of complex (a)  $[\text{Mn}(\text{L})(\text{OAc})]$ , (b)  $[\text{Co}(\text{L})(\text{OAc})]$ , (c)  $[\text{Ni}(\text{L})(\text{OAc})]$ , (d)  $[\text{Cu}(\text{L})(\text{OAc})]$  and (e)  $[\text{Zn}(\text{L})(\text{OAc})]$  at room temperature under  $\text{N}_2$ . The inset shows the growth of  $\pi \rightarrow \pi^*$  bands due to coordinated flavonolate.

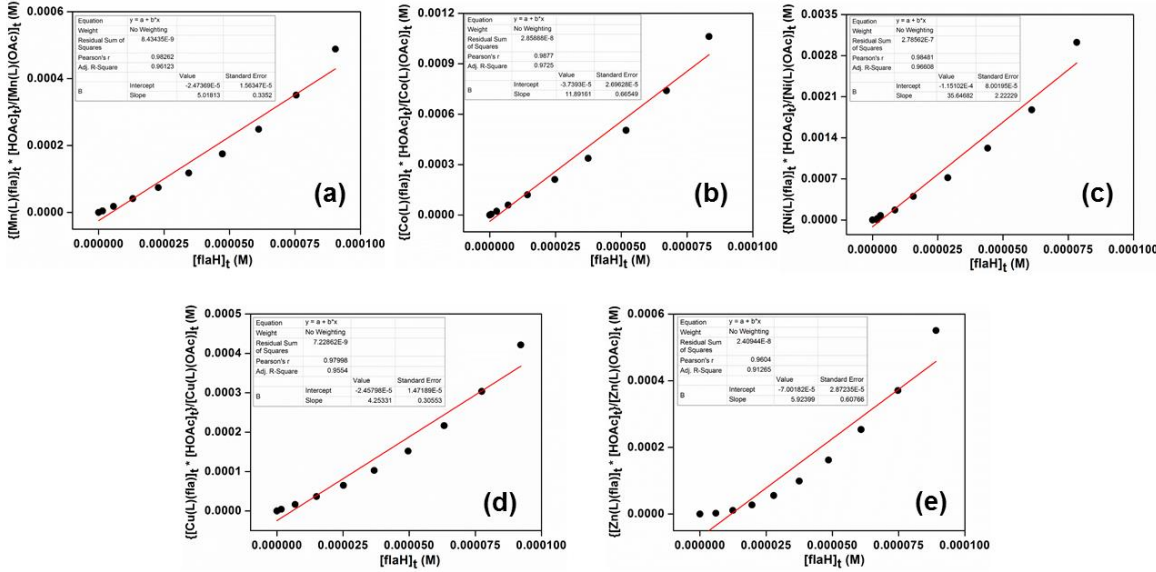


**Figure S37.** Plot of the corresponding  $\{[M(L)(\text{fla})]_t * [\text{HOAc}]_t\} / [\text{M}(L)(\text{OAc})]_t$  versus  $[\text{flaH}]_t$  to determine the formation constant ( $K_f$ ): (a) Mn (b) Co (c) Ni (d) Cu and (e) Zn. The slope of the linear fit represents the  $K_f$  values.

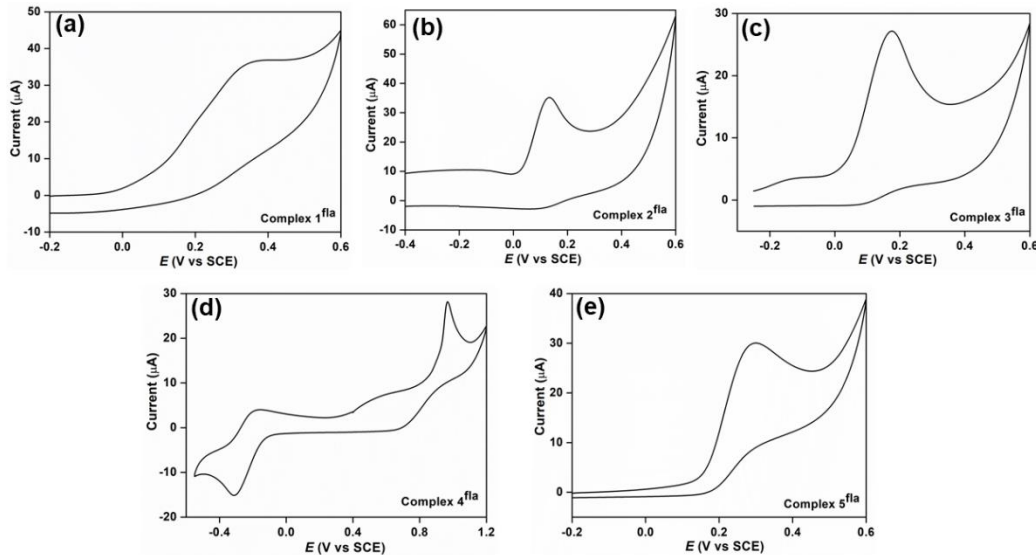


**Figure S38.** Cyclic voltammograms of the M(II)-flavonolato complexes in DMF: (a)  $[\text{Mn(L)}(\text{fla})]$  ( $1^{\text{fla}}$ ), (b)  $[\text{Co(L)}(\text{fla})]$  ( $2^{\text{fla}}$ ), (c)  $[\text{Ni(L)}(\text{fla})]$  ( $3^{\text{fla}}$ ), (d)  $[\text{Cu(L)}(\text{fla})]$  ( $4^{\text{fla}}$ ) and (e)  $[\text{Zn(L)}(\text{fla})]$  ( $5^{\text{fla}}$ ) (scan rate: 100 mV/s; supporting electrolyte:  $\text{KPF}_6$ ).

**Table S3:** GC-MS analysis at 70 °C in DMF

Catalyst	Product distributions (%)					Conversion (%)
	<i>o</i> -benzoylsalicylic acid (RT: 23.21)	2-hydroxybenzoic acid (RT: 10.93)	Benzoic acid (RT: 8.44)	2-hydroxy-N,N-dimethylbenzamide (RT: 12.54)	N,N-dimethylbenzamide (RT: 11.07)	
$[\text{Mn(L)}(\text{OAc})]$ ( $1^{\text{OAc}}$ )	23	n.d.	1	n.d.	5	29
$[\text{Co(L)}(\text{OAc})]$ ( $2^{\text{OAc}}$ )	4	4	21	5	59	84
$[\text{Ni(L)}(\text{OAc})]$ ( $3^{\text{OAc}}$ )	15	4	14	6	47	76
$[\text{Cu(L)}(\text{OAc})]$ ( $4^{\text{OAc}}$ )	17	n.d.	n.d.	1	n.d.	18
$[\text{Zn(L)}(\text{OAc})]$ ( $5^{\text{OAc}}$ )	31	1	1	n.d.	2	34

n.d. not detected

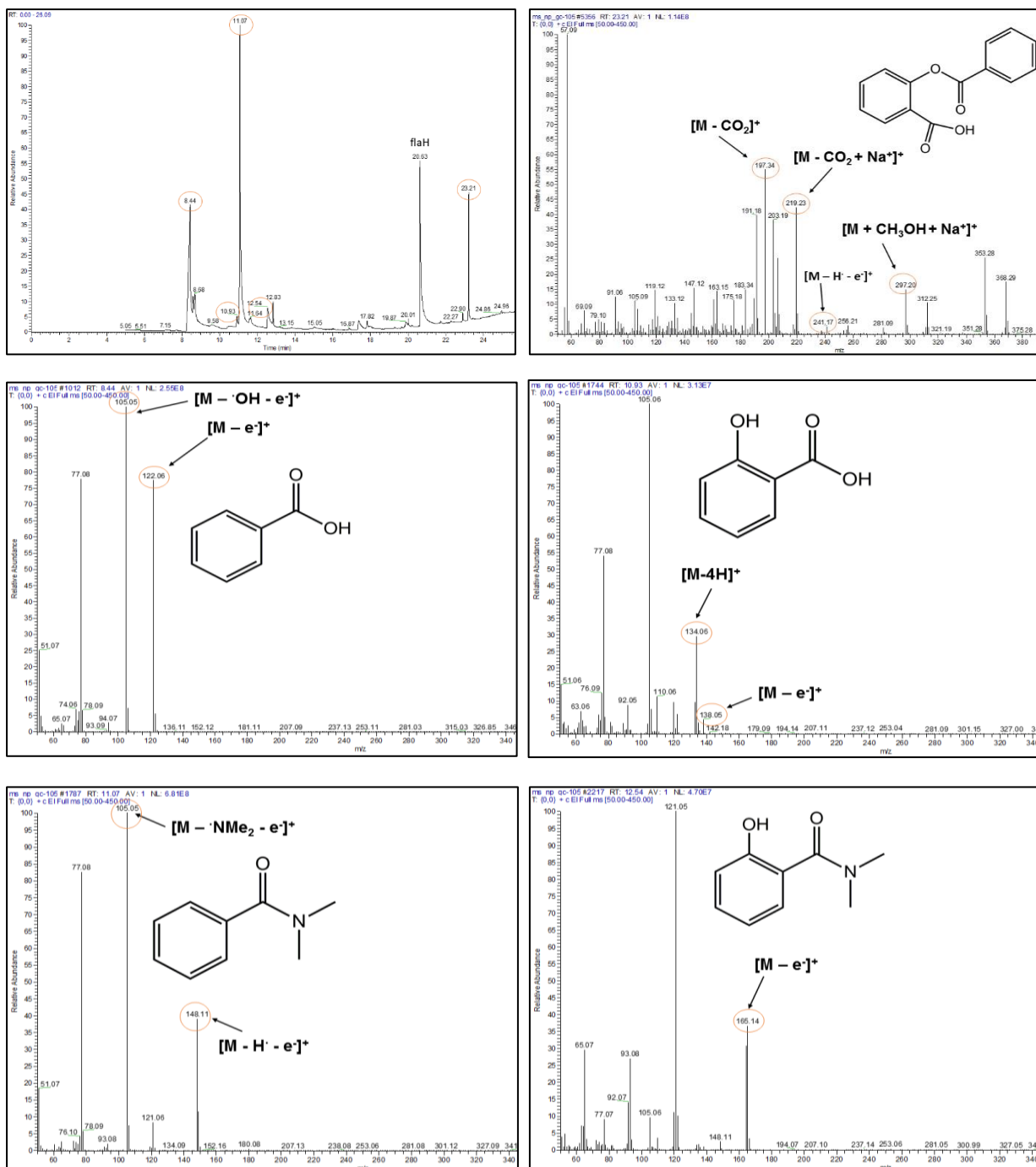


**Figure S39.** Representative gas chromatogram and the mass spectra (positive ion mode) of the products obtained from the catalysis with  $[\text{Ni}(\text{L})(\text{OAc})]$  (**3<sup>OAc</sup>**).

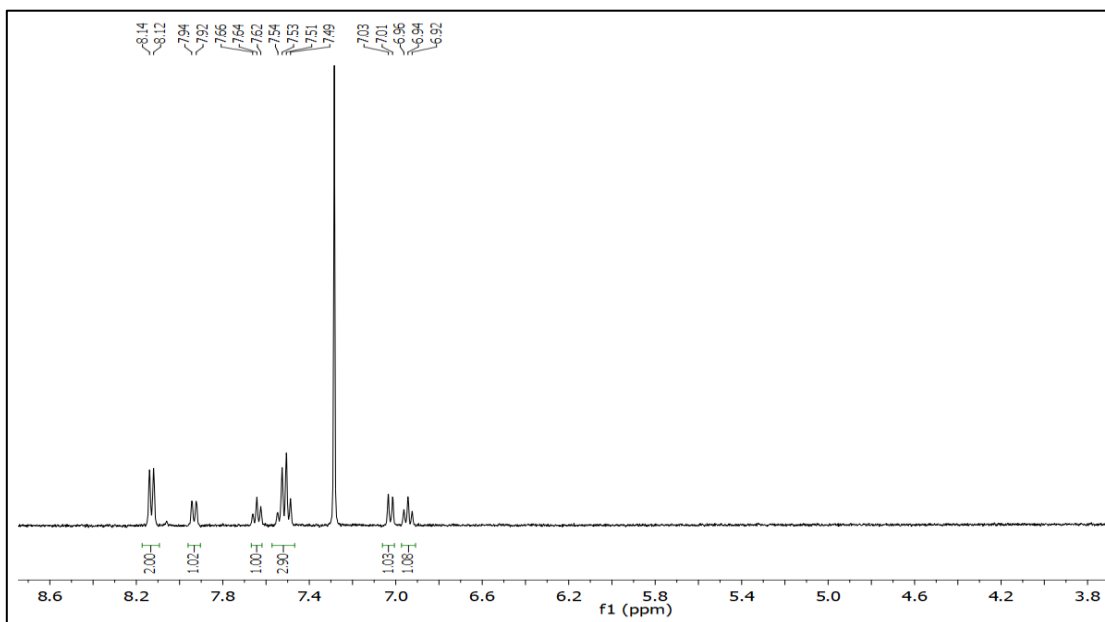


**Figure S40.**  $^1\text{H}$  NMR spectrum (in  $\text{CDCl}_3$ ) of the flavonol degraded products via dioxygenation catalysed by  $[\text{Co}(\text{L})(\text{OAc})] (\mathbf{2}^{0\text{Ac}})$ . Signals correspond to mixture of benzoic acid [ $\delta(\text{ppm}) = 8.13$  (d, 2H), 7.64 (t, 1H), 7.51 (t, 2H)] and salicylic acid [ $\delta(\text{ppm}) = 7.93$  (d, 1H), 7.51 (t, 1H), 7.02 (d, 1H), 6.94 (t, 1H)] in 50:50 ratio.

Table S4. Kinetic data for complex $[\text{Mn}(\text{L})(\text{OAc})] (\mathbf{1}^{0\text{Ac}})$							
Exp No.	T ( $^\circ\text{C}$ )	$[\text{O}_2]$ ( $10^{-3}\text{M}$ )	[flaH] ( $10^{-4}\text{ M}$ )	$[\text{Mn}(\text{L})(\text{OAc})]$ ( $10^{-6}\text{ M}$ )	$v_{\text{in}}$ ( $10^{-8}\text{Ms}^{-1}$ )	$k_3$ ( $10^5\text{M}^{-2}\text{s}^{-1}$ )	$k_3(\text{av})$ ( $10^5\text{M}^{-2}\text{s}^{-1}$ )
1	70	1.08	1	1	0.30	0.28	0.29
2	70	1.40	1	1	0.43	0.31	
3	70	1.72	1	1	0.52	0.30	
4	70	2.15	0.8	1	0.50	0.29	
5	70	2.15	1	1	0.60	0.28	
6	70	2.15	1.2	1	0.73	0.28	
7	70	2.15	1.4	0.5	0.48	0.32	
8	70	2.15	1.4	1	0.88	0.29	
9	70	2.15	1.4	1.5	1.33	0.29	
10	70	2.15	1.4	2.0	1.76	0.29	

Table S5. Kinetic data for complex $[\text{Co}(\text{L})(\text{OAc})] (\mathbf{2}^{0\text{Ac}})$							
Exp No.	T ( $^\circ\text{C}$ )	$[\text{O}_2]$ ( $10^{-3}\text{M}$ )	[flaH] ( $10^{-4}\text{ M}$ )	$[\text{Co}(\text{L})(\text{OAc})]$ ( $10^{-6}\text{ M}$ )	$v_{\text{in}}$ ( $10^{-8}\text{Ms}^{-1}$ )	$k_3$ ( $10^5\text{M}^{-2}\text{s}^{-1}$ )	$k_3(\text{av})$ ( $10^5\text{M}^{-2}\text{s}^{-1}$ )
1	70	1.08	1	1	6.45	5.97	6.17
2	70	1.40	1	1	8.68	6.20	
3	70	1.72	1	1	10.86	6.31	
4	70	2.15	0.8	1	10.48	6.09	
5	70	2.15	1	1	13.50	6.28	
6	70	2.15	1.2	1	16.47	6.38	
7	70	2.15	1.4	0.5	8.66	5.75	
8	70	2.15	1.4	1	18.85	6.26	
9	70	2.15	1.4	1.5	27.95	6.19	
10	70	2.15	1.4	2.0	37.62	6.25	

**Table S6.** Kinetic data for complex [Ni(L)(OAc)] (**3<sup>OAc</sup>**)

Exp No.	T (°C)	[O <sub>2</sub> ] (10 <sup>-3</sup> M)	[flaH] (10 <sup>-4</sup> M)	[Ni(L)(OAc)] (10 <sup>-6</sup> M)	v <sub>in</sub> (10 <sup>-8</sup> Ms <sup>-1</sup> )	k <sub>3</sub> (10 <sup>5</sup> M <sup>-2</sup> s <sup>-1</sup> )	k <sub>3</sub> (av) (10 <sup>5</sup> M <sup>-2</sup> s <sup>-1</sup> )
1	70	1.08	1	1	3.09	2.86	2.95
2	70	1.40	1	1	4.28	3.06	
3	70	1.72	1	1	5.25	3.05	
4	70	2.15	0.8	1	5.05	2.94	
5	70	2.15	1	1	6.32	2.94	
6	70	2.15	1.2	1	7.30	2.83	
7	70	2.15	1.4	0.5	4.6	3.06	
8	70	2.15	1.4	1	8.80	2.92	
9	70	2.15	1.4	1.5	13.10	2.90	
10	70	2.15	1.4	2.0	17.50	2.91	

**Table S7.** Kinetic data for complex [Cu(L)(OAc)] (**4<sup>OAc</sup>**)

Exp No.	T (°C)	[O <sub>2</sub> ] (10 <sup>-3</sup> M)	[flaH] (10 <sup>-4</sup> M)	[Cu(L)(OAc)] (10 <sup>-6</sup> M)	v <sub>in</sub> (10 <sup>-8</sup> Ms <sup>-1</sup> )	k <sub>3</sub> (10 <sup>5</sup> M <sup>-2</sup> s <sup>-1</sup> )	k <sub>3</sub> (av) (10 <sup>5</sup> M <sup>-2</sup> s <sup>-1</sup> )
1	70	1.08	1	1	0.20	0.19	0.19
2	70	1.40	1	1	0.26	0.19	
3	70	1.72	1	1	0.35	0.20	
4	70	2.15	0.8	1	0.33	0.19	
5	70	2.15	1	1	0.42	0.20	
6	70	2.15	1.2	1	0.50	0.19	
7	70	2.15	1.4	0.5	0.28	0.19	
8	70	2.15	1.4	1	0.57	0.19	
9	70	2.15	1.4	1.5	0.88	0.19	
10	70	2.15	1.4	2.0	1.18	0.20	

**Table S8.** Kinetic data for complex [Zn(L)(OAc)] (**5<sup>OAc</sup>**)

Exp No.	T (°C)	[O <sub>2</sub> ] (10 <sup>-3</sup> M)	[flaH] (10 <sup>-4</sup> M)	[Zn(L)(OAc)] (10 <sup>-6</sup> M)	v <sub>in</sub> (10 <sup>-8</sup> Ms <sup>-1</sup> )	k <sub>3</sub> (10 <sup>5</sup> M <sup>-2</sup> s <sup>-1</sup> )	k <sub>3</sub> (av) (10 <sup>5</sup> M <sup>-2</sup> s <sup>-1</sup> )
1	70	1.08	1	1	0.49	0.45	0.47
2	70	1.40	1	1	0.69	0.49	
3	70	1.72	1	1	0.84	0.49	
4	70	2.15	0.8	1	0.80	0.47	
5	70	2.15	1	1	1.00	0.47	
6	70	2.15	1.2	1	1.16	0.45	
7	70	2.15	1.4	0.5	0.68	0.45	
8	70	2.15	1.4	1	1.42	0.47	
9	70	2.15	1.4	1.5	2.05	0.45	
10	70	2.15	1.4	2.0	2.75	0.46	

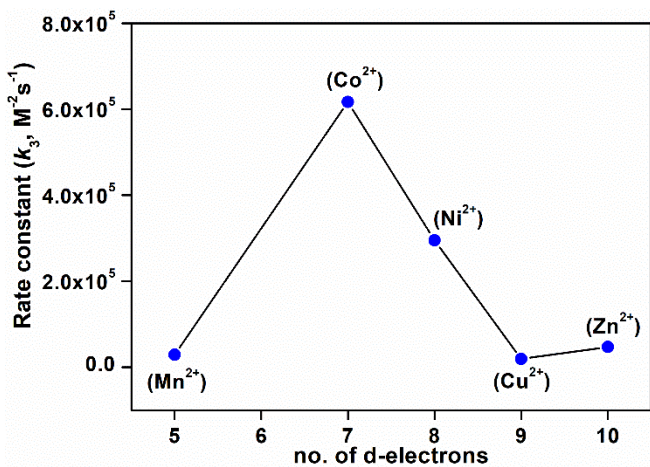


**Figure S41.** The plot of rate constants ( $k_3$ ) versus the number of d-electrons for the series of complexes  $\mathbf{1}^{\text{OAc}}\text{-}\mathbf{5}^{\text{OAc}}$ .

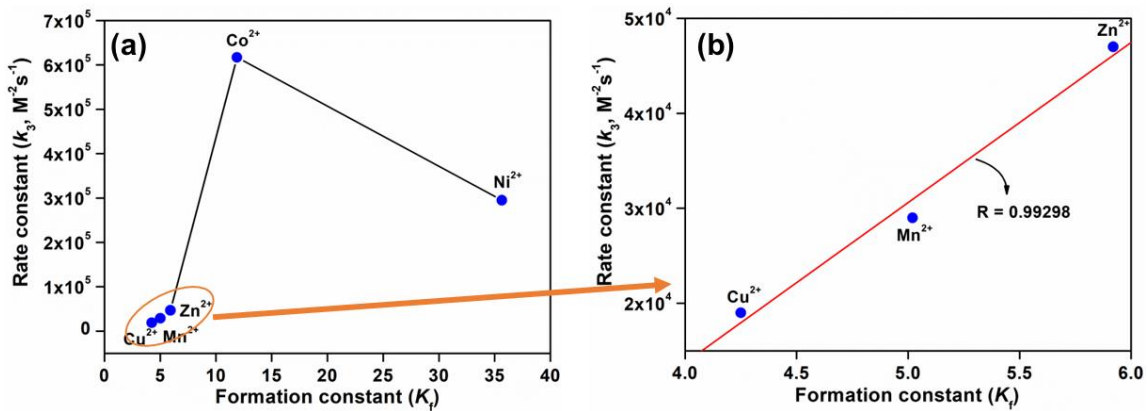


**Figure S42.** The plots of  $k_3$  versus the  $K_f$  values: (a) considering all five metal ions  $\text{Mn}^{2+}$ ,  $\text{Co}^{2+}$ ,  $\text{Ni}^{2+}$ ,  $\text{Cu}^{2+}$  and  $\text{Zn}^{2+}$ , (b) for the  $\text{Cu}^{2+}$ ,  $\text{Mn}^{2+}$  and  $\text{Zn}^{2+}$  ions. The red line in Figure b represents the linear fitting.

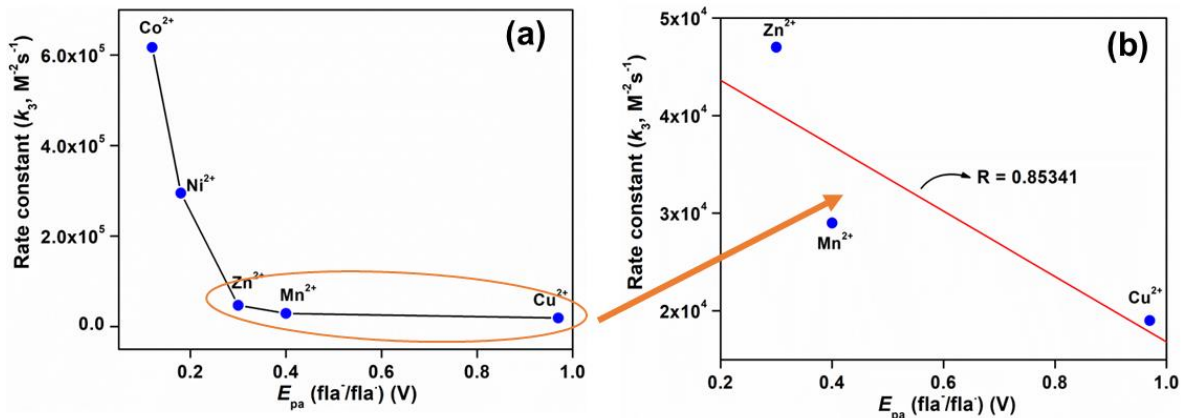


**Figure S43.** The plots of  $k_3$  versus the  $E_{\text{pa}}$  values: (a) considering all five metal ions  $\text{Mn}^{2+}$ ,  $\text{Co}^{2+}$ ,  $\text{Ni}^{2+}$ ,  $\text{Cu}^{2+}$  and  $\text{Zn}^{2+}$ , (b) for the  $\text{Cu}^{2+}$ ,  $\text{Mn}^{2+}$  and  $\text{Zn}^{2+}$  ions. The red line in Figure b represents the linear fitting.

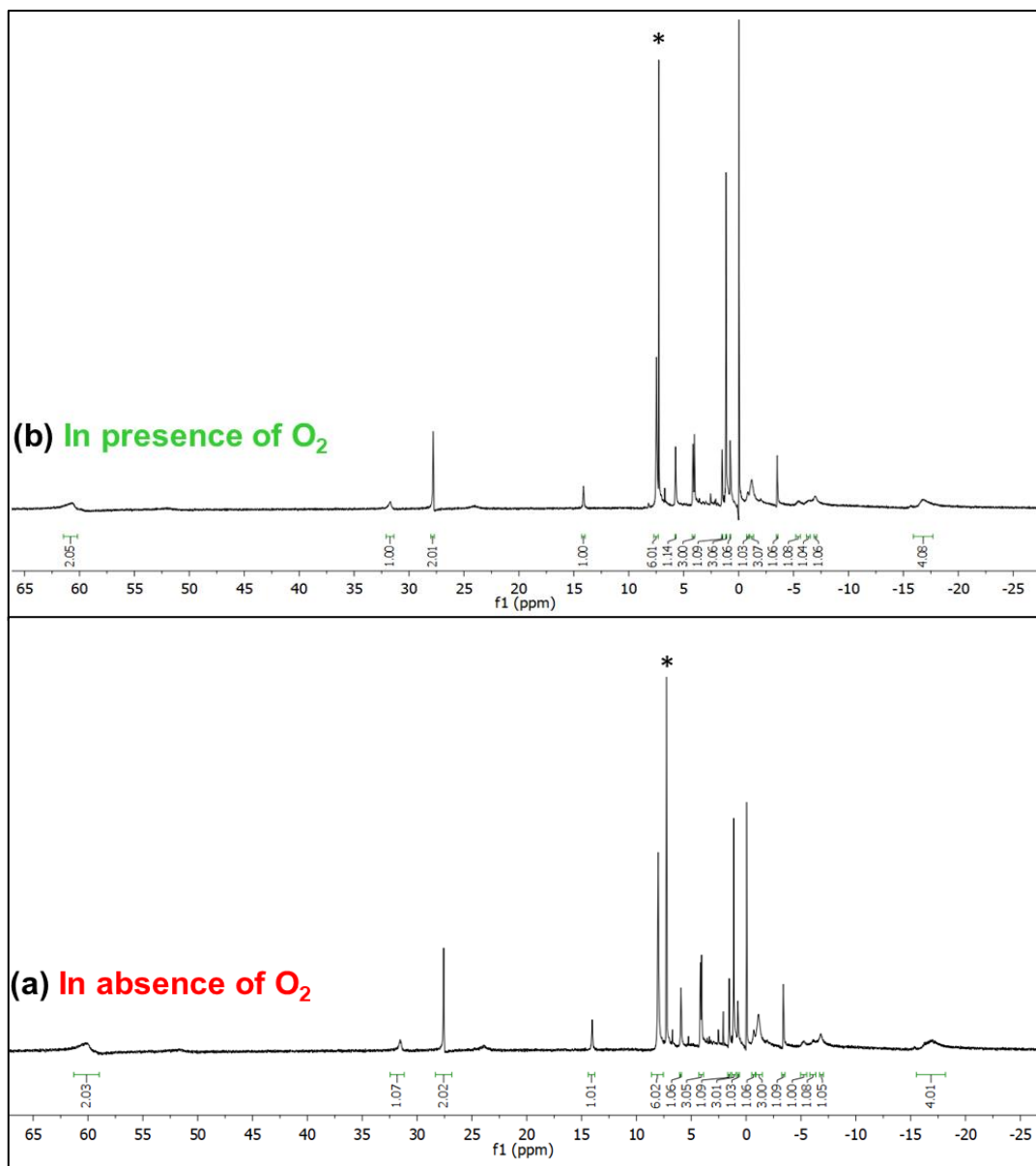


**Figure S44.** <sup>1</sup>H NMR spectra (400 MHz, 300 K, CDCl<sub>3</sub>) of complex [Co(L)(fla)] (**2**<sup>fla</sup>) in (a) absence and (b) presence of dioxygen.

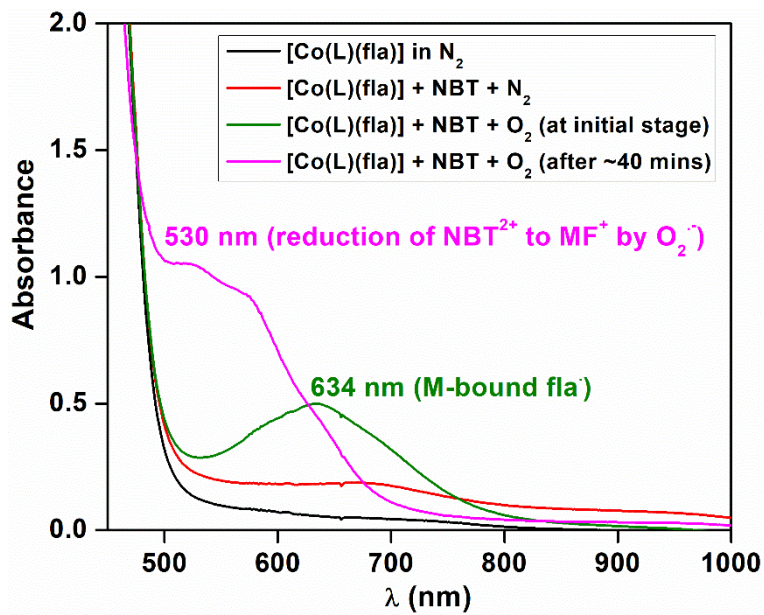


**Figure S45.** Spectral changes in the reaction of  $[Co(L)(fla)]$  with dioxygen in the presence of  $NBT^{2+}$  in DMF at  $70\text{ }^\circ C$ .

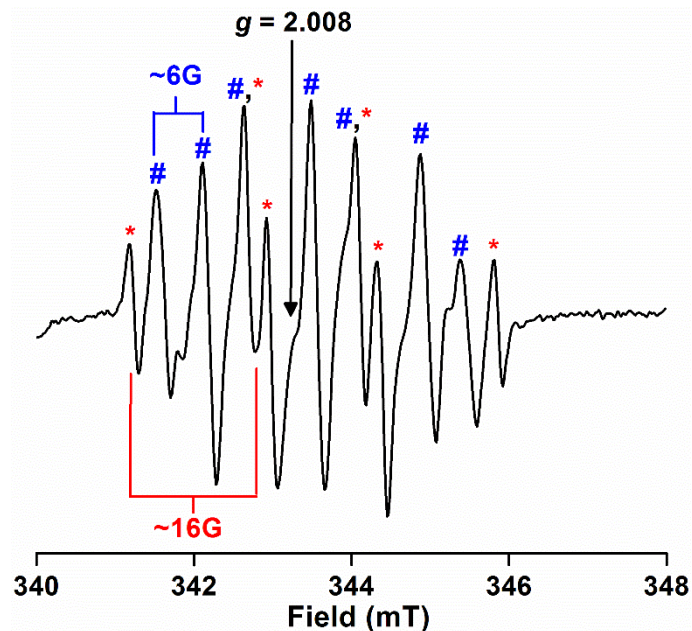


**Figure S46.** EPR spectrum of the reaction of  $[Co(L)(fla)]$  ( $2^{fla}$ ) with DMPO in the presence of  $O_2$  in DMF. The sample was prepared at  $70\text{ }^\circ C$ , and the spectrum was recorded at  $298\text{ K}$  (microwave frequency  $\sim 9.65\text{ GHz}$ ). The lines marked with  $*$  and  $\#$  correspond to signals for DMPO-O<sub>2</sub><sup>+</sup> and DMPO-OH species, respectively.